

# Display and quantitative assessment of distributions of earthquake focal mechanisms

Cliff Frohlich

Institute for Geophysics, University of Texas at Austin, Austin, TX 78759, USA. E-mail: cliff@utig.ig.utexas.edu

Accepted 2000 August 24. Received 2000 August 22; in original form 2000 May 30

## SUMMARY

This paper describes quantitative methods for evaluating the distribution of focal mechanism orientations of groups of earthquakes, and shows how to display this distribution on a triangle diagram. We present a  $\chi^2$ -based statistical test for determining whether two sets of focal mechanisms are drawn from distinct populations. We apply these methods to 3625 better-determined mechanisms for shallow earthquakes in the Harvard Centroid Moment Tensor (CMT) catalogue; we describe the distributions of mechanisms in the whole catalogue and for catalogue subsets in some specific tectonic environments. In addition, we explore the geographical locations of mechanisms with orientations that occur relatively infrequently, that is, mechanisms that are unlike thrust, normal, or strike-slip mechanisms. Such mechanisms are relatively rare along mid-ocean ridges and in oceanic subduction zones. The majority of these unusual mechanisms occur along plate boundaries where crustal thickness is highly variable, and in regions where the plate convergence direction becomes oblique and thus relative motion changes from convergence to transform motion.

**Key words:** earthquake source mechanism, statistical methods, stress distribution, tectonic stress.

## INTRODUCTION

Triangle diagrams (Frohlich 1992, 1996; Frohlich & Apperson 1992) are ternary graphs for plotting double-couple earthquake focal mechanisms; because the three vertices correspond to 'pure' strike-slip, normal, and thrust mechanisms (Fig. 1), the graphs are particularly useful for displaying the contrast of earthquake types observed in different tectonic environments. Triangle diagrams are one of several graphical methods for displaying groups of focal mechanisms, each with distinct advantages and disadvantages. For example, all double-couple mechanisms plot at the same location on the plot of Hudson *et al.* (1989), reducing its usefulness for tectonic analysis. Unlike triangle diagrams, the methods proposed by Riedesel & Jordan (1989), Hudson *et al.* (1989), Sipkin (1993, 1994) and Willemann (1993) all permit the display of non-double-couple mechanisms; however, this is not advantageous for many tectonic applications. Unlike triangle diagrams, the graphs proposed by Riedesel & Jordan (1989) and Sipkin (1993) preserve some information about the orientation of focal mechanisms; however, in some cases highly similar mechanisms plot at points far removed from one another on their graph. Willemann's (1993) method is novel but he does not focus attention on the display problem.

A major limitation of all these methods is that none of them naturally provides quantitative information characterizing the

clustering or rarity of various mechanism types—they do not provide information about the statistical distribution of a group of mechanisms. A second problem is that with each method, false clustering of mechanisms may occur on the display plot as a consequence of the projection that assigns a mechanism to a particular point on the graph. Both of these problems limit the usefulness of these graphical methods as the basis for quantitative tectonic analysis.

Thus, to address these problems we here explore several improvements to the triangle diagram methodology. First, for any set of double-couple mechanisms, we present a quantitative method to evaluate the relative frequency—the ratio of the number of mechanisms observed of any particular type to the number expected in a hypothetical catalogue where mechanisms have *T*-, *B*- and *P*-axes distributed uniformly in all directions over the focal sphere. We apply a natural gridding procedure to divide the triangle diagram into mutually exclusive subregions; plotting the relative frequencies within the subregions, rather than points representing the individual mechanisms, is one way to avoid the false clustering problem. However, for situations where it is desirable to plot individual mechanisms, we describe a new projection where the false clustering is significantly reduced in comparison to other commonly used methods. The gridding procedure is also the basis for a formal statistical test to evaluate whether different sets of mechanisms are drawn from distinct populations.

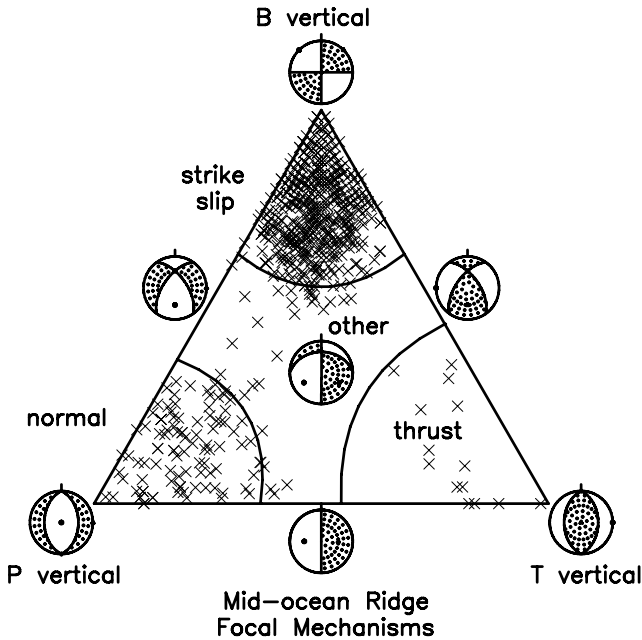


**Figure 1.** Triangle diagram for displaying the distribution of double-couple focal mechanisms. Mechanisms with vertical  $T$ ,  $B$  and  $P$  axes plot at the vertices of the triangle. Curved lines surround regions where  $T$ ,  $B$  and  $P$  axes lie within  $40^\circ$ ,  $30^\circ$  and  $30^\circ$  of the vertical, respectively. Frohlich (1992) suggested the defining mechanisms that plot in these regions as thrust, strike-slip, and normal; he defined all remaining mechanisms as ‘other’. In this figure, the X symbols indicate the mechanisms for 637 reliably determined CMT mechanisms for earthquakes occurring along mid-ocean ridges (see text and Fig. 5), plotted using eq. (3). Whilst this shows that most mid-ocean ridge earthquakes cluster near the normal and strike-slip vertices, the intense clustering makes it difficult to evaluate quantitatively the distribution.

To illustrate the application of these improvements, we apply them to the centroid moment tensor (CMT) catalogue and address two specific questions. First, whilst it is qualitatively obvious that strike-slip and normal earthquakes are common along mid-ocean ridges and thrust earthquakes are common in subduction zones, how strong is this clustering quantitatively? Second, while the majority of earthquakes possess mechanisms that are thrust, strike-slip, or normal, how common are mechanisms that are unlike any of these three types? Moreover, in what geographical locations and tectonic environments are these relatively infrequent mechanisms likely to occur?

## METHODS

### Octants and triangle diagrams

For any double-couple focal mechanism, the azimuth and plunge angles of the principal axes  $T$ ,  $B$  and  $P$  completely describe its orientation. However, these angles are not independent; because  $T$ ,  $B$  and  $P$  are orthogonal, a law of geometry requires that their plunge angles  $\delta_T$ ,  $\delta_B$  and  $\delta_P$  (that is, the angles with respect to the horizontal plane) satisfy

$$\sin^2 \delta_T + \sin^2 \delta_B + \sin^2 \delta_P = 1. \quad (1)$$

Furthermore, if we consider the vertical components of the three axes:

$$\begin{aligned} x &= |\sin \delta_T|, \\ y &= |\sin \delta_P|, \\ z &= |\sin \delta_B|. \end{aligned} \quad (2)$$

Eq. (1) becomes  $x^2 + y^2 + z^2 = 1$ , the equation of a sphere; this is actually an octant (i.e. a quarter-hemisphere) because, as defined in eq. (2),  $x$ ,  $y$ , and  $z$  are positive. This octant representation for focal mechanisms is important for describing quantitatively which mechanisms are common or rare. This is because if double-couple focal mechanisms are produced by a random process that generates all possible orientations with equal likelihood, the resulting distribution is isotropic and thus uniform on this octant.

Whilst the octant representation is mathematically natural, a projection akin to a map projection is necessary for displaying mechanisms graphically on a flat surface such as paper or a computer screen. Kaverina *et al.* (1996) have suggested a projection to a distorted triangle which preserves areas on the octant. However, most geoscientists have instead used the azimuthal gnomonic projection (Richardus & Adler 1972). This projects the octant onto an equilateral triangle of height  $H$ ; the horizontal and vertical distances  $h_G$  and  $v_G$  from the central point (where  $\sin^2 \delta_T = \sin^2 \delta_B = \sin^2 \delta_P = 1/3$ ) are

$$h_G = H2^{1/2} \cos \delta_B \sin \psi [3(\sin \theta_0 \sin \delta_B + \cos \theta_0 \cos \delta_B \cos \psi)], \quad (3)$$

$$v_G = H2^{1/2} (\cos \theta_0 \sin \delta_B - \sin \theta_0 \cos \delta_B \cos \psi) / [3(\sin \theta_0 \sin \delta_B + \cos \theta_0 \cos \delta_B \cos \psi)].$$

Here,  $\psi$  is the angle such that  $\psi = -45^\circ + \tan^{-1}(\sin \delta_T / \sin \delta_P)$  and  $\theta_0$  is  $35.26^\circ$  [i.e.  $\theta_0 = \sin^{-1}(1/3^{1/2})$ ]. Note that eq. (3) differs slightly from the erroneous previous versions of these formulae published in Frohlich & Apperson (1992) and Frohlich (1992).

Unfortunately, the azimuthal gnomonic projection is not an equal-area projection (Fig. 2). The area projected on the triangle exceeds that on the octant by a factor  $F_G$ , which increases away from the central point (where  $F_G = 1$ ):

$$F_G = 3^{3/2} / (\sin \delta_T + \sin \delta_B + \sin \delta_P)^3, \quad (4)$$

$$F_G = 3^{3/2} / (x + y + z)^3. \quad (5)$$

The distortion is significant (Fig. 2 and Table 1); at the triangle vertices,  $F_G = 5.2$ .

Other projections besides eq. (3) are possible, even if one maintains an equilateral triangle as the projected surface. For example, a mathematically very simple projection is to set the horizontal and vertical distances  $h_S$  and  $v_S$  from the central point by

$$h_S = H(\sin^2 \delta_T - \sin^2 \delta_P) / 3^{1/2}, \quad (6)$$

$$v_S = H(\sin^2 \delta_B - 1/3).$$

This projection has the desirable property that small circles centred at the points corresponding to all three of the vertices are projected as straight lines on the triangle diagram (Fig. 2). However, this also is not an equal-area projection, and the distortion is severe (Table 1). Areas projected onto the triangle

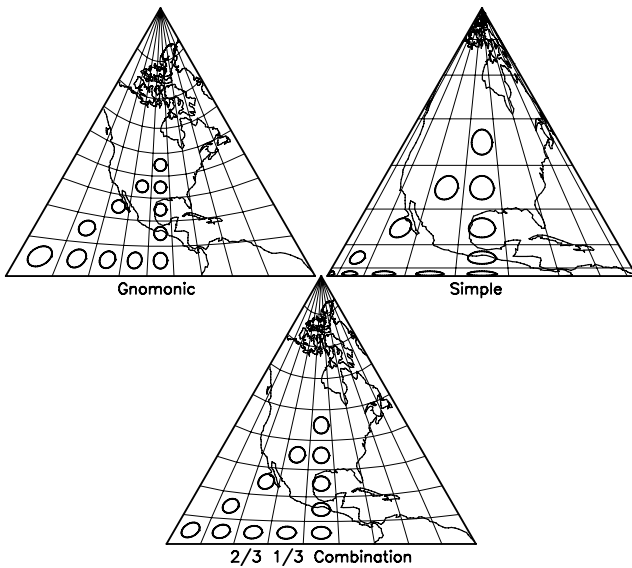


**Figure 2.** Areal distortion in triangle diagrams produced by three different projections: (upper left) azimuthal gnomonic projection (eq. 3); (upper right) simple projection (eq. 6; see text); and (lower diagram) the combined projection (eq. 9; see text), where plotted points are one-third of the distance between azimuthal gnomonic and simple projection. Each diagram shows the projection of a quarter-hemisphere of the Earth's surface ( $0^\circ - 90^\circ\text{N}$ ;  $140^\circ - 50^\circ\text{W}$ ) and includes latitude and longitude lines at  $10^\circ$  intervals. To illustrate the distortion, plots include projections of circles with radii of 300 km at various locations on the Earth's surface.

become smaller away from the central point; the areal growth factor  $F_S$  is

$$F_S = 3^{3/2} \sin \delta_T \sin \delta_B \sin \delta_P, \quad (7)$$

$$F_S = 3^{3/2} xyz. \quad (8)$$

At the vertices,  $F_S$  is zero.

For later use, we mention a third class of projections, formed by combining the azimuthal gnomonic projection of eq. (3) and the simple projection of eq. (6). For any number  $f$  between 0 and 1, the horizontal and vertical distances  $h_C$  and  $v_C$  for this combined projection are

$$h_{C-f} = fh_G + (1-f)h_S, \quad (9)$$

$$v_{C-f} = fv_G + (1-f)v_S.$$

**Table 1.** Comparison of areal distortion encountered when triangle diagrams are constructed using three different projections and no correction is made for distortion. Table values are minimum and maximum values of  $RF_{\Delta-\text{raw}}$  (eq. 11) within the  $N^2$  subtriangles in a diagram, determined by generating 1 000 000 randomly orientated focal mechanisms (see text). Thus, if the minimum and maximum values of  $RF_{\Delta-\text{raw}}$  were both 1.0, there would be 1 000 000/ $N^2$  mechanisms within each of the  $N^2$  subtriangles.

$N$	$N^2$	Gnomonic		Simple		Combined	
		Min	Max	Min	Max	Min	Max
3	$3^2$	0.63	1.19	0.54	1.66	0.99	1.00
6	$6^2$	0.44	1.51	0.43	3.15	0.90	1.05
9	$9^2$	0.39	1.60	0.41	4.62	0.84	1.07
12	$12^2$	0.34	1.65	0.40	6.12	0.82	1.10

As before, this is not an equal-area projection; however, when  $f$  is  $2/3$  it is significantly closer than either eq. (3) or eq. (6) (see Table 1). We have found no simple closed formula for the areal growth factor  $F_C$ .

### Relative frequencies and subtriangles

In a catalogue containing  $M$  focal mechanisms, how can we measure whether mechanisms with particular  $T$ ,  $B$  and  $P$  plunge angles  $\delta_T$ ,  $\delta_B$  and  $\delta_P$  are common or rare? Because isotropically distributed mechanisms would be uniformly distributed on the octant, a natural approach is to consider a small circle of arbitrary radius  $\alpha$  surrounding the point  $(x, y, z)$  given by eq. (2), and then count the number of mechanisms in the catalogue which fall within an angular distance  $\alpha$  on the octant, that is, those for which  $xx+yy+zz \geq \cos \alpha$ . If there are  $m_\alpha$  such mechanisms, then the small circle subtends a fraction  $4(1 - \cos \alpha)$  of the octant, and a measure of the relative frequency of mechanisms is

$$RF_\alpha = m_\alpha / [4M(1 - \cos \alpha)]. \quad (10)$$

Thus,  $RF_\alpha = 1$  if the density of mechanisms near  $(x, y, z)$  is the same as a uniform, isotropic distribution of mechanisms. Of course, eq. (10) has to be adjusted appropriately if the circle around  $(x, y, z)$  intersects the boundary of the octant.

For evaluating distributions, eq. (10) can sometimes be inconvenient because no combination of circles covers the octant with mutually exclusive subregions. There are various possible methods for partitioning the octant (e.g. see Kagan & Jackson 1998); however, on a triangle diagram, a straightforward way is to divide the triangle diagram into subtriangles and count the number of mechanisms in each subtriangle (Fig. 3). For

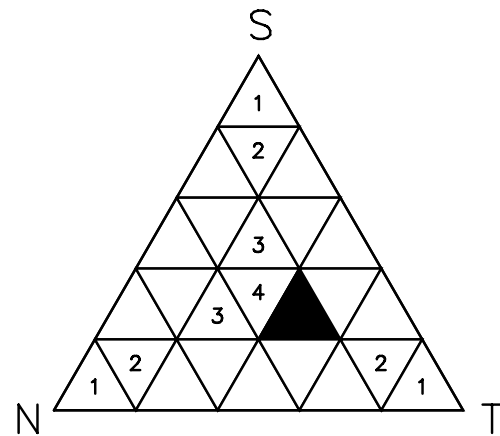


**Figure 3.** The mathematics of subtriangles. We can divide a triangle of height  $H$  into  $N^2$  subtriangles by drawing equally spaced lines a distance  $H/N$  apart, parallel to each of the three sides. To label each subtriangle we use three integers  $k_N, k_S, k_T$ , selected so that the triangle lies between the lines which are a distance  $H(k_N-1)/N$  and  $Hk_N/N$  from the  $N$  vertex, a distance  $H(k_S-1)/N$  and  $Hk_S/N$  from the  $S$  vertex and a distance  $H(k_T-1)/N$  and  $Hk_T/N$  from the  $T$  vertex. For plotting triangles, it is useful to know which indexes correspond to upward-pointing and downward-pointing triangles. For upward-pointing subtriangles,  $k_N, k_S$ , and  $k_T$  satisfy  $k_N + k_S + k_T = 2N + 1$ . For downward-pointing subtriangles, they satisfy  $k_N + k_S + k_T = 2N + 2$ . For example, in this figure  $N$  is 5 and the labels  $k_N, k_S$  and  $k_T$  for the darkened subtriangle are 4, 4 and 3, respectively. It is upward pointing since  $4 + 4 + 3 = 2 \times 5 + 1$ .

example, suppose there are  $M$  focal mechanisms in a catalogue which we plot on a triangle diagram with  $N^2$  subtriangles. If  $m_{ijk}$  lie within the subtriangle indexed by  $i, j$  and  $k$ , an estimate of the relative frequency is

$$RF_{\Delta\text{-raw}}(i, j, k) = N^2(m_{ijk}/M). \quad (11)$$

However, for comparisons,  $RF_{\Delta\text{-raw}}$  is biased because none of the projections described above are equal-area projections. The most nearly equal-area projection is the combined projection (eq. 9), when  $f$  is approximately  $2/3$ . For example, if  $N$  is 9 and the diagram is divided into 81 subtriangles, among these 81 subtriangles the maximum distortion is only 16 per cent (Table 1). The bias is less for smaller values of  $N$ .

A more precise approach is to weight individually each focal mechanism, with the weight determined by the areal growth factors  $F_G$  or  $F_S$ . In this case the sums corresponding to both the  $m_{ijk}$  and the  $M$  must be weighted sums, for example,

$$w_{ijk} = \sum_{\text{sub}\Delta} F_G,$$

$$W_M = \sum_{\text{all}} F_G,$$

where the sum for  $w_{ijk}$  is over the individual subtriangle, and the sum for  $W_M$  is over all  $M$  mechanisms. Then,

$$RF_{\Delta\text{-weighted}} = N^2(w_{ijk}/W_M). \quad (12)$$

This method is most practical for the azimuthal gnomonic projection, since  $F_S$  for the simple projection goes to zero at the triangle vertices.

### Comparing distributions of mechanisms

Regardless of which method is chosen to divide the octant into subregions, the partitioning makes it possible to apply a  $\chi^2$ -test to evaluate whether a set  $S_1$  of focal mechanisms is drawn from a particular fiducial distribution. Suppose, for example, that there are  $M_1$  mechanisms in  $S_1$  distributed over  $N^2$  subregions, and the model predicts that the fraction of mechanisms in the  $k$ th subregion is  $f_k$ . Then if  $S_1$  has  ${}_1n_k$  mechanisms in the  $k$ th subregion, the  $\chi^2$  statistic is

$$\chi^2 = \sum_{k=1}^{N^2} \frac{({}_1n_k - f_k M_1)^2}{f_k M_1}. \quad (13)$$

There are  $N^2 - 1$  degrees of freedom, and a table of the percentiles of the  $\chi^2$  distribution can be used to evaluate how different  $S_1$  is from the fiducial distribution.

Alternatively, one can test whether two sets  $S_1$  and  $S_2$  are drawn from distinct populations. In this case we assume that the most likely fiducial distribution is the intersection of the sets  $S_1$  and  $S_2$ , so that

$$f_k = \frac{{}_1n_k + {}_2n_k}{M_1 + M_2} \quad (14)$$

and

$$\chi^2 = \sum_{k=1}^{N^2} \frac{({}_1n_k - f_k M_1)^2}{f_k M_1} + \frac{({}_2n_k - f_k M_2)^2}{f_k M_2}. \quad (15)$$

There are  $2N^2 - 2$  degrees of freedom.

## RESULTS

### Distribution of mechanisms in the entire CMT catalogue

The most extensive compilation of earthquake focal mechanisms is the Harvard CMT catalogue, which includes 16 410 mechanisms for earthquakes occurring between 1977 and October 1999 (e.g. Dziewonski & Woodhouse 1983; Dziewonski *et al.* 2000). For this study, we selectively eliminated events with reported focal depths exceeding 30 km. We also eliminated mechanisms that did not reliably meet the standards proposed by Frohlich & Davis (1999), that is, those with non-double-couple components greater than 40 per cent ( $f_{\text{clvd}} > 0.2$ ), those with relative errors greater than 15 per cent, and those where one or more of the six moment tensor elements was fixed during the inversion. Of the 16 410 mechanisms in the catalogue, only 8687 had focal depths of 30 km or less; of these, only 3625 (42 per cent) met the Frohlich & Davis (1999) reliability standards.

Clearly, the orientations of mechanisms for these 3625 selected shallow earthquakes are not distributed uniformly and isotropically (Fig. 4). Frohlich (1992) suggested categorizing thrust, strike-slip and normal mechanisms as those with  $T$ ,  $B$  and  $P$  axes within  $40^\circ$ ,  $30^\circ$  and  $30^\circ$ , respectively, of the vertical. By this definition 48 per cent of the CMT mechanisms are thrusts, 30 per cent are strike-slip and 11 per cent are normal. These three categories include 89 per cent of all CMT mechanisms, even though together the three groups only occupy 50 per cent of the octant; that is, 25 per cent of the octant lies within the thrust region, and 13 per cent within both the normal and strike-slip regions.

However, the highest frequencies do not occur exactly at the vertices. The most numerous mechanisms are thrusts which occur along the bottom edge of the diagram near  $A_T$  (subscript T denotes thrust), where the  $T$ -axis plunge is  $65^\circ$ ; indeed, 1272 mechanisms, or more than one third of all selected mechanisms, occur within  $15^\circ$  of  $A_T$ . At  $A_T$  the peak relative frequency  $RF_z$  is about 12 (Table 2); that is, the frequency is 12 times higher than would occur if mechanisms were distributed uniformly and isotropically. The highest density of normal mechanisms occurs near  $A_N$  (subscript N denotes normal), where the peak  $RF_z$  is about 2. The highest density of strike-slip mechanisms occurs at the vertex; where  $RF_z$  is about 7.

Why aren't the thrust and normal peaks at the vertices? The observations in Fig. 4 are generally consistent with the Anderson theory of faulting (Anderson 1942; Scholz 1990). Near a free surface and in the absence of static friction the Anderson theory predicts that dip angles of strike-slip, thrust and normal faults would be  $90^\circ$ ,  $45^\circ$  and  $45^\circ$ , respectively. However, when the static friction coefficient is non-zero, the dip angle  $\beta$  is steeper along normal faults (about  $55^\circ$  from Fig. 4) and shallower along thrust faults (about  $25^\circ$  from Fig. 4).

### Distribution of mechanisms in typical subduction or mid-ocean ridge regions

When mechanisms from similar tectonic environments are grouped together, they exhibit characteristic patterns on the triangle diagrams. Along oceanic ridge transform regions (RT in Fig. 5), most mechanisms are strike-slip or normal and there is a near-absence of thrust and 'other' types. Of the 637 mechanisms in Figs 1 and 6(a), 78 per cent are strike-slip,

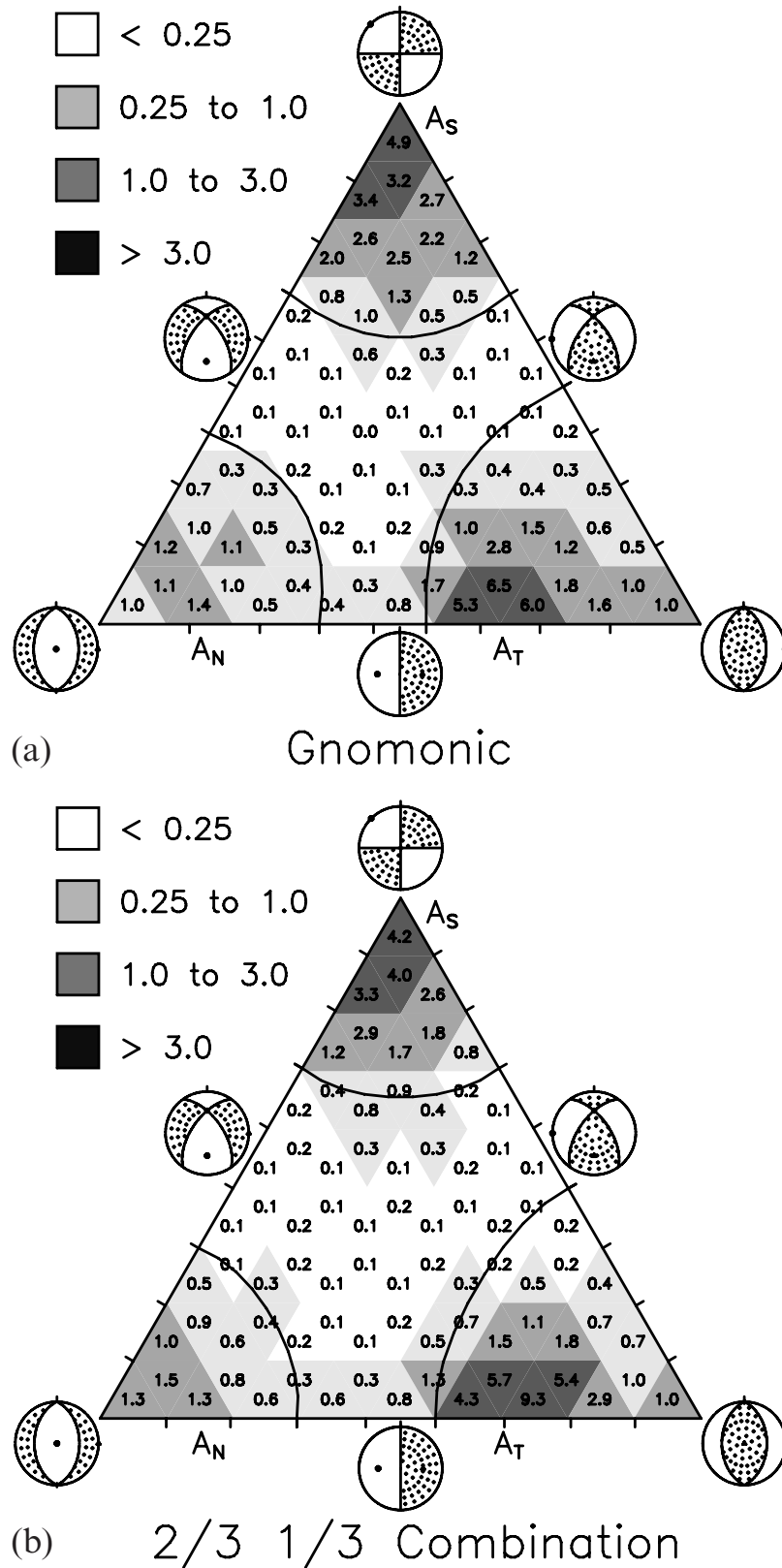


**Figure 4.** Distribution of relative frequencies for shallow-focus Harvard CMT mechanisms. Data are 3625 reliably determined mechanisms (see text); plotted numbers and shading indicate relative frequencies in each of 81 triangular subregions. In (a) data are plotted using the azimuthal gnomonic projection (eq. 3) with relative frequency determined using eq. (12). In (b) data are plotted using the combination projection (eq. 6 with  $f=2/3$ ) and relative frequency is determined using eq. (11). There are peaks in relative frequencies near regions labelled  $A_N$ ,  $A_T$  and  $A_S$ ; these correspond to normal, thrust and strike-slip faults with dips of about  $55^\circ$ ,  $20^\circ$  and  $90^\circ$ , respectively. Note that the regions of higher frequencies are nearly all within about  $20^\circ$  (or two tick marks along edge of the triangle) of  $A_N$ ,  $A_T$  and  $A_S$ . The highest relative frequencies occur in the subtriangles near  $A_T$ , reaching 6.5 in (a) and 9.3 in (b).

**Table 2.** Relative frequencies of various focal mechanism types, as determined using  $RF_z$  (eq. 10), modified where necessary to account for octant boundaries. The  $1/2$  radius is calculated only when the frequency distribution is relatively symmetric about a clearly defined peak; it is determined from the average levels in  $\pm 1^\circ$  doughnut-shaped regions surrounding the peak. For example, on the octant, the average level in the region falling between  $8^\circ$  and  $10^\circ$  from the thrust peak  $A_T$  is 6.1, or half of the maximum of 12.2; thus the  $1/2$  radius is  $9^\circ$ .

Mechanism type	centre, small circle			radius $\alpha$	$RF_z$	$1/2$ radius
	$\delta_T$	$\delta_B$	$\delta_P$			
Entire CMT catalogue—3625 reliable mechanisms (see Fig. 4)						
Thrust peak $A_T$	$65^\circ$	$0^\circ$	$25^\circ$	$2.5^\circ$	12.2	$9^\circ$
Strike-slip peak $A_S$	$0^\circ$	$90^\circ$	$0^\circ$	$2.5^\circ$	7.2	$11^\circ$
Normal peak $A_N$	$10^\circ$	$0^\circ$	$80^\circ$	$2.5^\circ$	1.9	—
Triangle centre	$35.3^\circ$	$35.3^\circ$	$35.3^\circ$	$10^\circ$	0.13	—
Ridge transform regions—637 reliable mechanisms (see Figs 1, 5 and 6a)						
Strike-slip peak	$0^\circ$	$90^\circ$	$0^\circ$	$3.5^\circ$	16.0	$15.5^\circ$
Normal peak	$6^\circ$	$0^\circ$	$84^\circ$	$3.5^\circ$	3.8	—
Uniform perpendicular subduction—178 reliable mechanisms (see Figs 6b and 7)						
Thrust peak	$65^\circ$	$0^\circ$	$25^\circ$	$3.5^\circ$	45.2	$5.5^\circ$

17 per cent are normal, 2 per cent are thrusts, while only 3 per cent are ‘other’. At the vertex where the frequency of strike-slip mechanisms is greatest, the relative frequency reaches 16 times uniform with a half-width of  $15.5^\circ$  (Table 2).

In contrast, where subducting crust is of uniform thickness, where both subducting and overriding plates are oceanic, and where the convergence direction is nearly perpendicular (UPS in Figs 7 and 6b), thrust mechanisms dominate, with a few normal and strike-slip mechanisms associated with seismicity along the outer rise. For many oceanic subduction zones, the central portion of the triangle diagram shows a near-absence of ‘other’ mechanisms. For example, in Fig. 6(b), 1 per cent are strike-slip, 6 per cent are normal, 89 per cent are thrusts, while only 4 per cent are ‘other’. The subtriangle gridding scheme

indicates that mechanisms are concentrated most strongly within two of the diagram’s 36 subtriangles, where their relative frequency is about 12 times greater than the level of a uniform distribution. In fact, the subtriangle gridding is insensitive to peak frequencies; the more peak-focused analysis (Table 2) indicates that the peak frequency is actually a factor of 45 above uniform, and the peak has a half-width of about  $5.5^\circ$ .

#### Infrequent mechanisms in the centre of the triangle diagram

Among the better-determined mechanisms in the CMT catalogue there are 402 ‘other’ mechanisms (about 11 per cent), with  $T$ ,  $B$  and  $P$  axes all far enough from the vertical that they do

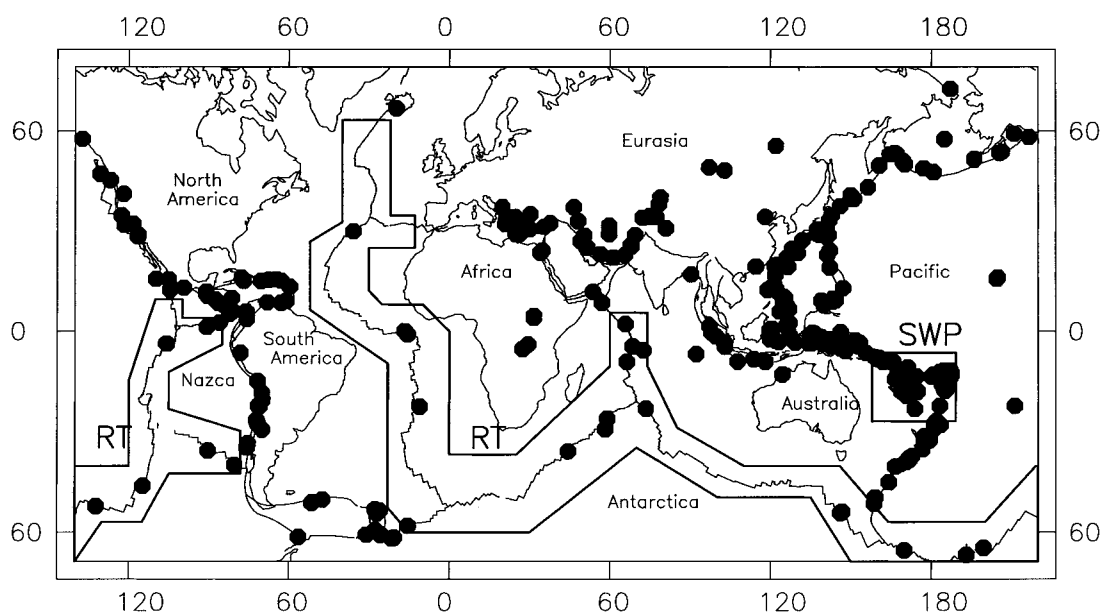


**Figure 5.** (Top) Global distribution of ‘other’ mechanisms. Filled symbols indicate locations of 402 reliably determined shallow-focus CMT classified as ‘other’ in Fig. 1. Region labelled RT shows ridge-transform region containing earthquakes plotted in Fig. 1; box labelled SWP indicates the southwest Pacific area detailed in Fig. 7.

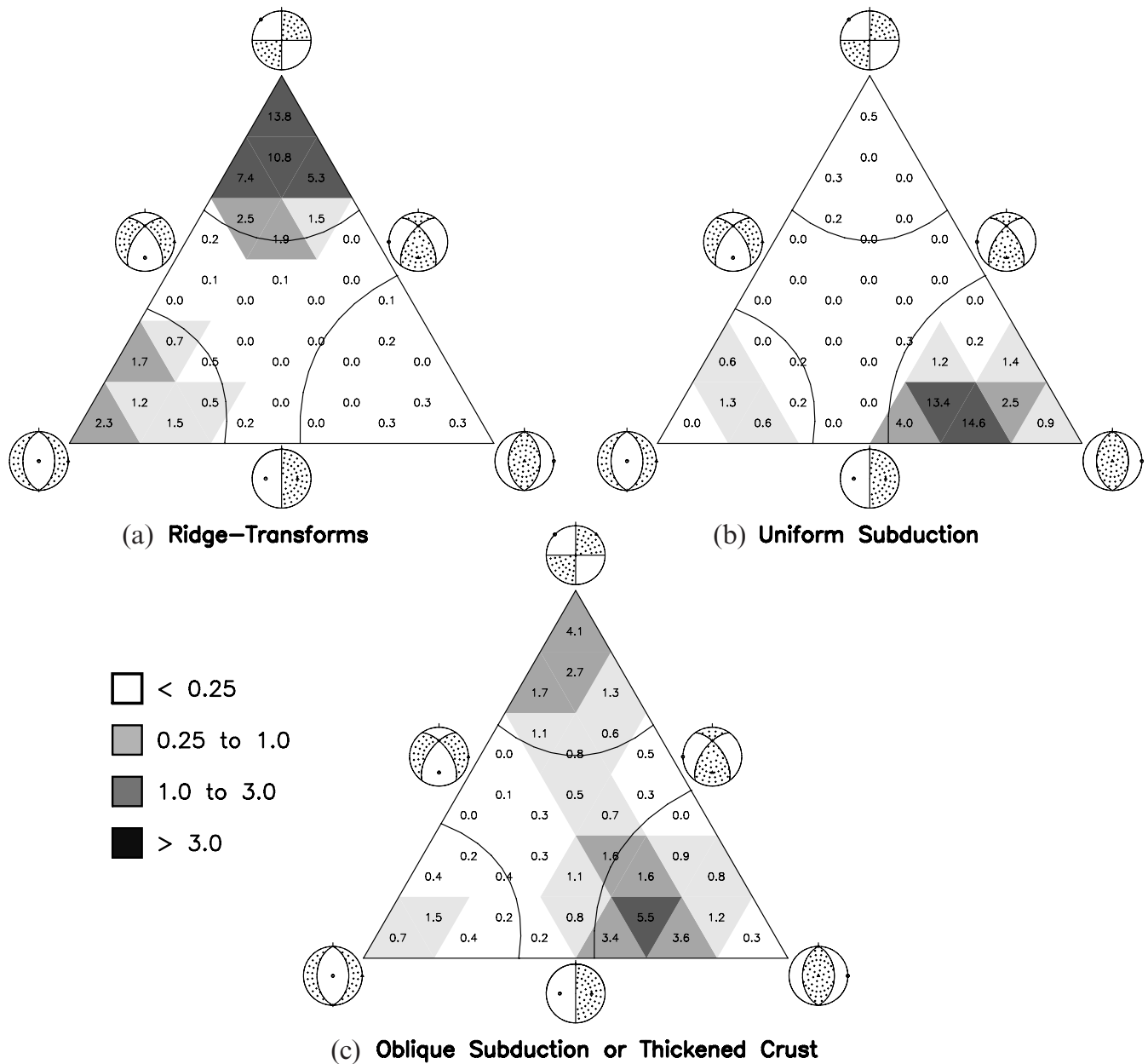


**Figure 6.** Characteristic focal mechanism patterns in three tectonic regimes. Shading and plotted numbers within subtriangles indicate relative frequency of well-determined focal mechanisms for: (a) ridge transforms—637 earthquakes within region RT in Fig. 5; (b) ordinary subduction—178 earthquakes within UPS boxes in Fig. 7; (c) oblique/transverse subduction or thickened crust—233 earthquakes within the OST and TC boxes in Fig. 7. Projection for all plots is azimuthal gnomonic (eq. 3), and relative frequencies are determined separately for subtriangles in each earthquake group using eq. (12).

not qualify as thrust, strike-slip, or normal mechanisms. What is responsible for these mechanisms, and why aren't all mechanisms near the peaks predicted by Anderson's theory?

Some of the centre-of-diagram mechanisms may be attributable to statistical variations introduced by Harvard's inversion process. At least three recent studies have investigated these variations (Helffrich 1997; Frohlich & Davis 1999; Kagan 2000) and found that statistical variations can be large for outliers in the CMT catalogue. However, for selected, better-determined mechanisms, such as those investigated in the present study, all three investigations concluded that systematic errors in axial orientations are usually  $20^\circ$  or less. The ridge transform and subduction zone data in Figs 6(a) and (b) support

this conclusion, since in both plots the peaks observed have half-widths smaller than  $20^\circ$ . Thus, it is likely that the majority of the 402 'other' mechanisms are real.

Where, geographically, do these centre-of-diagram mechanisms occur? On a global scale (Fig. 5) they are not concentrated; however, closer inspection indicates that most occur in a few specific tectonic environments. Of the 402 'other' mechanisms, about one-quarter occur in regions where subduction becomes oblique and relative plate motion becomes transverse (for examples, see Bilich *et al.* 2000). For example, in the southwest Pacific (Fig. 7), Australia-Pacific plate motion becomes transverse in the northern Tonga arc near Samoa, in the southern New Hebrides arc near Matthew and Hunter Islands,

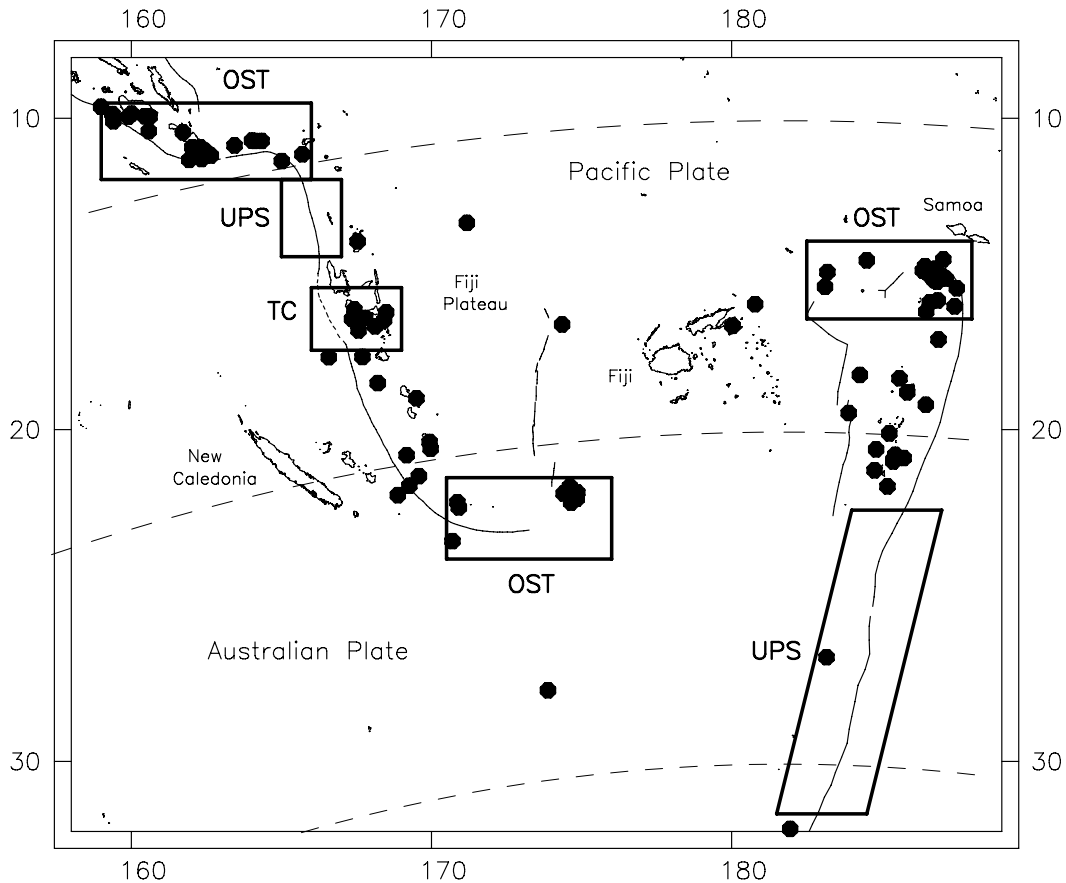


**Figure 7.** Locations of 'other' mechanisms in the southwest Pacific region. Boxes labelled OST indicate regions where relative plate motion (dashed lines) produces oblique subduction/transverse motion at the plate boundary; box labelled TC indicates where thickened crust of the D'Entrecasteaux Ridge subducts beneath the Pacific plate; boxes labelled UPS indicate two regions of uniform, perpendicular subduction—where subducting crust is relatively uniform and the convergence direction is nearly perpendicular.

and also at the junction of the New Hebrides and Solomon arcs. These three regions alone, labelled OST in Fig. 7, account for 51, or 13 per cent, of the 402 'other' mechanisms.

Of course, not all the mechanisms in oblique subduction regions occur in the centre of the diagram. However, the  $\chi^2$ -tests (eqs 13 and 15) demonstrate that the 233 mechanisms in Fig. 6(c) form a distribution that is distinctly different both from the distribution represented by the 3625 selected mechanisms from the Harvard CMT catalogue and from the 178 mechanisms from a typical subduction region (Fig. 6b). In particular, suppose we partition the mechanisms by using an azimuthal gnomonic triangle diagram divided into 36 sub-triangles. If we use the frequencies observed for selected Harvard CMT mechanisms as the fiducial model, eq. (13) gives a  $\chi^2$  of 147.3. If we compare the sets of 233 and 178 mechanisms using eq. (15), the  $\chi^2$  is 133.0. Tables of the  $\chi^2$  distribution indicate that both are significant at greater than the 99th percentile level.

Another large group of centre-of-diagram mechanisms (about 35 per cent) occurs along plate boundaries where the crustal thickness changes abruptly, often because oceanic crust subducts beneath thicker continental crust. For example, there are about 25 such mechanisms along the west coasts of Central and South America; they also occur near Greece in the Mediterranean, and in south-Central Alaska. These mechanisms often occur where plate boundaries lie near large islands

such as New Guinea, the Philippines, and Taiwan. Finally, they may occur in situations where the thicker crust is not continental; for example, there are nine 'other' mechanisms where thickened crust of the D'Entrecasteaux Ridge subducts beneath the Pacific plate (region TC in Fig. 7).

The remaining centre-of-diagram mechanisms are distributed in several different tectonic environments. About 10 per cent occur along mid-ocean ridges (see Fig. 5), another 10 per cent lie near triple-junctions and about 10 per cent are situated in the interiors of plates, well away from any plate boundary.

## DISCUSSION AND CONCLUSIONS

This paper describes quantitative methods for evaluating distributions of sets of double-couple focal mechanisms, such as might be obtained from sampling the Harvard CMT catalogue. The methods compare the observed frequency of mechanisms to the frequency in a hypothetical catalogue of uniformly, isotropically distributed mechanisms. Triangle diagrams (Figs 4 and 6) provide a straightforward means for displaying the frequency distribution, with shading, numerical labels, or contour lines indicating the relative frequencies of mechanisms within various portions of the diagram.

In this paper we have proposed a gridding method (Fig. 3) which divides the triangle diagram into sub-triangles and which can be used to partition sets of focal mechanisms into distinct



subgroups. This partitioning allows the application of statistical tests based on the  $\chi^2$  statistic (eqs 13 and 15) to evaluate whether different sets of mechanisms arise from distinct populations.

We also propose a new combination projection (eq. 9) for plotting triangle diagrams, which is more nearly equal-area than the azimuthal gnomonic projection (eq. 3). The azimuthal gnomonic projection is superior for many purposes because it is easier to manipulate quantitatively and thus to correct for the areal distortion; however, the combination projection is useful if one wishes to plot symbols for individual mechanisms, or display raw counts without correction for distortion. A Fortran program that plots graphs such as Figs 4(a) and (b) is available from the author upon request.

It will come as little surprise that these methods demonstrate that the great majority of shallow earthquakes in the CMT catalogue have thrust, strike-slip, or normal mechanisms; however, there is a significant portion (11 per cent) that have mechanisms which plot in the centre of the triangle diagram, well away from the thrust, strike-slip, or normal vertices. These central mechanisms occur only rarely along mid-ocean ridges and in well-behaved oceanic subduction zones (Figs 6a and b). More than half of them occur within two environments: along plate boundaries where the crustal thickness is highly variable; and along plate boundaries where the convergence direction is oblique, and relative motion changes from convergence to transform (see Bilich *et al.* 2000).

#### ACKNOWLEDGMENTS

Discussions with numerous participants at a Penrose Conference in Puerto Plata, Dominican Republic in January 1999 strongly influenced this paper. I also thank Yann Kagan, George Helffrich, Steven Ward and an anonymous reviewer who made suggestions which helped to improve this work.

#### REFERENCES

Anderson, E.M., 1942. *The Dynamics of Faulting*, 1st edn, Oliver and Boyd, Edinburgh.  
 Bilich, A., Frohlich, C. & Mann, P., 2000. Global seismicity characteristics of subduction-to-strike-slip transitions, *J. geophys. Res.*, in press.

Dziewonski, A.M. & Woodhouse, J.H., 1983. Studies of the seismic source using normal-mode theory, in *Earthquakes: Observation, Theory and Interpretation*, pp. 45–137, eds Kanamori, H. & Boschi, E., North-Holland, New York.  
 Dziewonski, A.M., Ekstrom, G. & Maternovskaya, N.N., 2000. Centroid-moment tensor solutions for January–March, 1999, *Phys. Earth planet. Inter.*, **118**, 1–11.  
 Frohlich, C., 1992. Triangle diagrams: ternary graphs to display similarity and diversity of earthquake focal mechanisms, *Phys. Earth planet. Inter.*, **75**, 193–198.  
 Frohlich, C., 1996. Cliff's nodes concerning plotting nodal lines for P, Sh and Sv, *Seism. Res. Lett.*, **67**, 16–24.  
 Frohlich, C. & Apperson, K.D., 1992. Earthquake focal mechanisms, moment tensors, and the consistency of seismic activity near plate boundaries, *Tectonics*, **11**, 279–295.  
 Frohlich, C. & Davis, S.D., 1999. How well constrained are well-constrained T, B, and P axes in moment tensor catalogs?, *J. geophys. Res.*, **104**, 4901–4910.  
 Helffrich, G.R., 1997. How good are routinely determined focal mechanisms? Empirical statistics based on a comparison of Harvard, USGS and ERI moment tensors, *Geophys. J. Int.*, **131**, 741–750.  
 Hudson, J.A., Pearce, R.G. & Rogers, R.M., 1989. Source type plot for inversion of the moment tensor, *J. geophys. Res.*, **94**, 765–774.  
 Kagan, Y.Y., 2000. Temporal correlations of earthquake focal mechanisms, *Geophys. J. Int.*, **143**, 881–897.  
 Kagan, Y.Y. & Jackson, D.D., 1998. Spatial aftershock distribution: effect of normal stress, *J. geophys. Res.*, **103**, 24 453–24 467.  
 Kaverina, A.N., Lander, A.V. & Prozorov, A.G., 1996. Global creep distribution and its relation to earthquake-source geometry and tectonic origin, *Geophys. J. Int.*, **125**, 249–265.  
 Richardus, R. & Adler, R.K., 1972. *Map Projections*, North-Holland, Amsterdam.  
 Riedesel, M.A. & Jordan, T.H., 1989. Display and assessment of seismic moment tensors, *Bull. seism. Soc. Am.*, **79**, 85–100.  
 Scholz, C.H., 1990. *The Mechanics of Earthquakes and Faulting*, Cambridge University Press, New York.  
 Sipkin, S.A., 1993. Display and assessment of earthquake focal mechanisms by vector representation, *Bull. seism. Soc. Am.*, **83**, 1871–1880.  
 Sipkin, S.A., 1994. Errata: display and assessment of earthquake focal mechanisms by vector representation, *Bull. seism. Soc. Am.*, **84**, 954.  
 Willemann, R.J., 1993. Cluster analysis of seismic moment tensor orientations, *Geophys. J. Int.*, **115**, 617–634.